

# Finite element simulation of pole vaulting

Sven Drücker<sup>1</sup> · Konrad Schneider<sup>2</sup> · Navneet-Kaur Ghothra<sup>2</sup> · Swantje Bargmann<sup>3</sup>

Published online: 11 October 2017

© The Author(s) 2017. This article is an open access publication

**Abstract** Pole vaulting is one of the most spectacular disciplines in athletics. The evolution of world record heights is strongly influenced by the development of advanced poles and subsequent materials. Employing advanced, load-adjusted composites has resulted in a steady increase of the world record height. This study provides a framework for finite element simulations of pole vaulting with focus on the initial and boundary conditions as well as finite element choices. The influence of the pole bending stiffness on the achievable height is systematically simulated. Higher effective bending stiffness leads to higher pole vaulting heights. However, if a certain stiffness is exceeded, the vaulter will not be able to bend the pole enough which leads to failed attempts.

**Keywords** Pole vaulting · Simulation · Finite element method

✉ Sven Drücker  
sven.druecker@tuhh.de

Konrad Schneider  
konrad.schneider@tuhh.de

Navneet-Kaur Ghothra  
navneet.ghothra@tuhh.de

Swantje Bargmann  
bargmann@uni-wuppertal.de

<sup>1</sup> Institute of Polymer Composites, Hamburg University of Technology, Denickestr. 15, 21073 Hamburg, Germany

<sup>2</sup> Institute of Continuum Mechanics and Materials Mechanics, Hamburg University of Technology, Eißendorfer Str. 42, 21073 Hamburg, Germany

<sup>3</sup> Chair of Solid Mechanics, University of Wuppertal, Gaußstr. 20, 42119 Wuppertal, Germany

## 1 Introduction

Pole vaulting is an astonishing sport where athletes use poles as an auxiliary equipment to clear the bar at heights of 5–6 m and more. Risen from a purpose driven technique, e.g., overcoming castle walls during siege, crossing irrigation ditches [1] and transport [2], pole vaulting has become one of the most spectacular and high-tech disciplines at the Olympic games. It is a dynamic, elegant and fascinating sport.

To clear the bar, pole vaulters need to transfer the kinetic energy of the approach into potential energy via the pole. Two factors determine the success of a vault: (1) physical abilities of the athlete (speed, strength and springiness) and (2) properties of the pole (low weight and ability to store and return energy in the most efficient way).

In times where the physical abilities of the athletes reach their limits, the pole and, thus, the material it is made of, becomes a key factor. Figure 1 depicts the development of the world record in pole vaulting over time.

In the early 20th century, bamboo poles were utilized which are light but also very stiff and, thus, not able to transfer the kinetic energy from the approach in an efficient manner. In the 1940s, aluminum and steel led to new world records—however, these materials show high stiffness as well and therefore did not significantly improve the vaulting height. In the beginning of the 1960s, lightweight fiber-reinforced plastics (with lower bending stiffness) became increasingly popular. They allow large elastic deflections. As a consequence, they are able to transfer more energy resulting in a more pronounced catapult effect. In the following years, the world record steadily rose due to improved fiber arrangements and vaulting techniques. In the 1990s, a new plateau of nearly 6.15 m was reached. This indicates that human physiology and

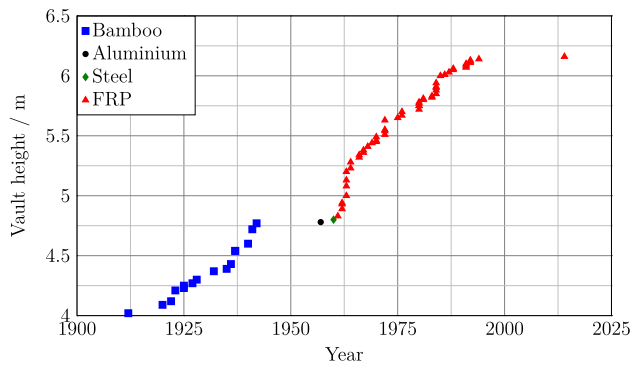


**Fig. 1** World record in pole vaulting over time with different materials (data from Hirn [3])

current materials may have reached a limit and enhancements of the pole's material are necessary to further improve the world record. The aim of this work is to provide a finite element (FE) model allowing for simulation aided pole design.

## 2 Model specifications

FE simulations of the pole vaulting process were conducted with the commercial FE code ABAQUS 6.14. The initial boundary value problem of the dynamic equation of motion was solved with an implicit time integration method under consideration of finite deformations. Exemplary FE models of the pole and the vaulter were obtained and generated in ABAQUS/CAE. To capture the kinematics of the pole vault procedure, a setting was employed that couples pole and vaulter allowing for a relative motion.

### 2.1 Finite element model of the vaulter

A comprehensive overview of the mechanics of pole vaulting can be found in Frère et al. [4] describing the process in four steps: run-up, take-off, pole bending and pole straightening. A crucial part in the jumping process simulation is the description of the vaulter. Muscle work of the vaulter increases the performance [5, 6]. In addition, the moment exerted on the pole by the vaulter influences the vaulting performance [7]—elite vaulters bend the pole such that its effective length<sup>1</sup> relative to the original length is reduced by ca. 30% [8]. As stated by Ekevad and Lundberg [9], a modeling approach representing the vaulter by a point mass with a fixed position relative to the pole is not sufficient. The complex motion in combination with muscle work needs to be considered.

<sup>1</sup> The effective length of the pole is referred to as the end to end distance.

Hubbard [10] applied a model of the vaulter consisting of three rigid segments representing different parts of the body. Ekevad and Lundberg [11] extended this approach to six segments in a 2D setting, sequentially connected by joints: forearm, upper arm, head, trunk, thigh and shank (cf. Fig. 2).

The two arms and legs were represented by one equivalent segment. A summary of the properties of the segments is shown in Table 1. In this paper, we extend the approach of Ekevad and Lundberg [11] by additionally accounting for a joint at the neck.

An exemplary motion of a vaulter was obtained by analyzing videos of a German elite pole vaulter<sup>2</sup>. Specific frames of the video were taken to represent different phases of the vault process. With the aid of CAD software several measurements were taken for each phase to describe the position of the vaulter's body segments. In accordance with the planar motion of the segments model, a side view was considered in the videos<sup>3</sup>. The motion was described relative to the upper pole tip. Thus, it can be used in simulations with poles of different lengths. To do so, three coordinate systems were introduced as shown in Fig. 2. First, the global coordinate system  $x$ - $y$  was fixed and located at the lower tip of the pole. Second, a relative coordinate system  $x_1$ - $y_1$  was established at the upper tip of the pole. In addition, a relative coordinate system  $x_2$ - $y_2$  was utilized with an origin coinciding with the previous one. This coordinate system rotates to maintain the  $x_2$ -axis tangential to the pole. The measured quantities are:

- Angle  $\varphi$  between ground and a line connecting the tips of the pole,
- Height  $h_p$  of upper pole tip,
- Angle  $\theta_0$  of the rotated coordinate system  $x_2$ - $y_2$ ,
- Angle  $\theta_1$  between the coordinate system  $x_2$ - $y_2$  and segment A, and
- Angles  $\theta_2$  to  $\theta_6$  between the segments A to F.

The angles  $\theta_i$  between the body segments of the reference pole vault over time are plotted in Fig. 3. A linear interpolation was performed between the discrete values.

At a second stage, the body was reduced to a point mass (center of gravity) with  $m = 80$  kg. Thus, the significant effort to control the individual segments of the vaulter with muscle torques is avoided allowing more computational time on material modeling. The position of the mass center  $\mathbf{x}_m$  in the coordinate system  $x_2$ - $y_2$  was calculated from the measured angles in each phase by

<sup>2</sup> The results of our simulations were extracted from the motion of one vaulter. To receive more general results for a specific pole, the variation of the motion of each vaulter as well as between different vaulters should be taken into account.

<sup>3</sup> The rotation of the pole to the side was not taken into account as the influence of movements out of the 2D plane was marginal [12].

**Fig. 2** Model of the vaulter based on Ekevad and Lundberg [11]

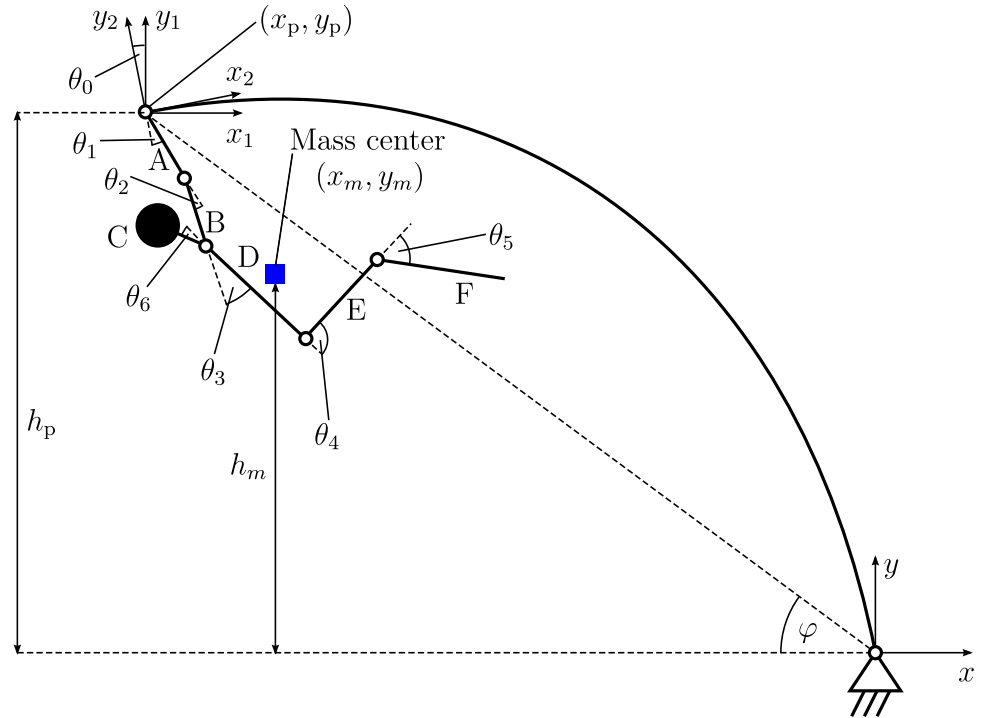


**Table 1** Properties of segments of vaulter model (data from [11])

Symbol	Segment	Length/mm	Mass/kg
A	Forearm	363	3.52
B	Upper arm	343	4.48
C	Head	332	6.48
D	Trunk	526	39.8
E	Thigh	447	16.0
F	Shank	521	9.76

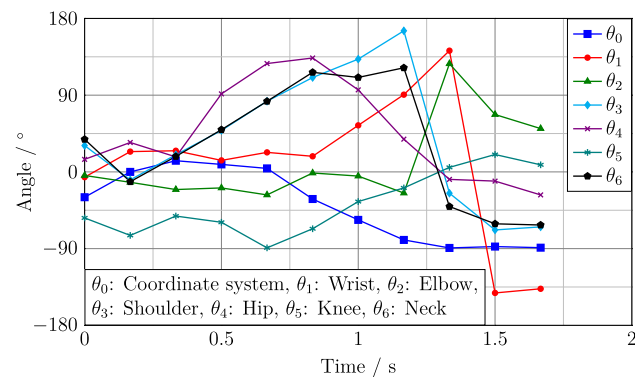


**Fig. 3** Body segment angles in reference pole vault. Those are used as input during the FE simulations

$$\mathbf{x}_m = \begin{bmatrix} x_m \\ y_m \end{bmatrix} = \frac{\sum_{i=A}^F \mathbf{x}_i m_i}{\sum_{i=A}^F m_i}, \quad (1)$$

where  $\mathbf{x}_i$  is the position of the mass center of the  $i$ th segment of the body and  $m_i$  is the mass of the  $i$ th segment. The point mass moves relative to the pole in coordinate system  $x_2$ - $y_2$  applying ABAQUS' connector elements (cf. Sect. 2.3). The different phases of the vault and the position of the mass center (blue square) are illustrated in Fig. 4.

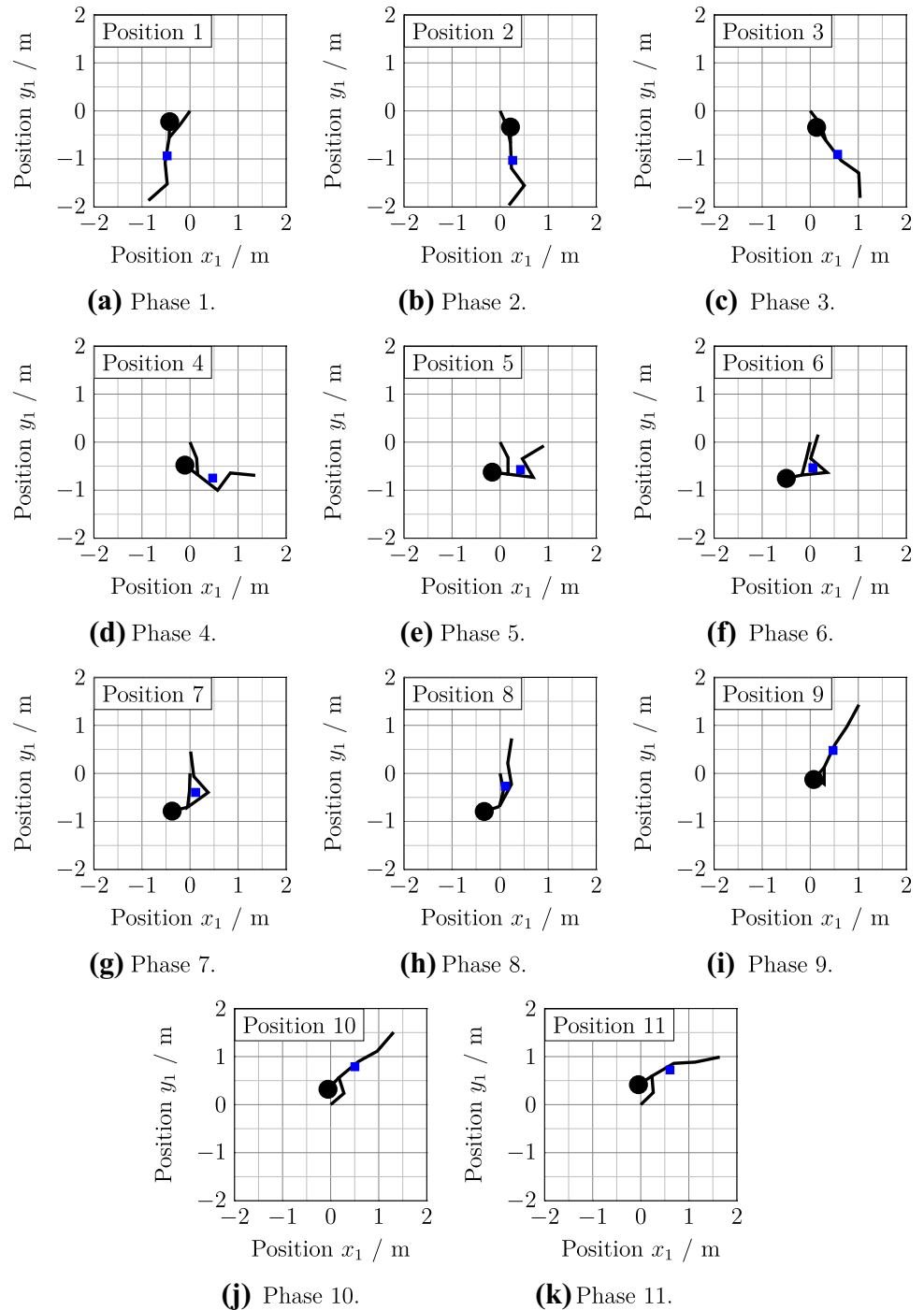
We employed two variables during the pole vault to trigger the relative motion of the point mass: the pole angle  $\varphi$  from take-off to the instance of maximum pole bending, and the relative height  $h_{m,rel}$  of the point mass from maximum pole bending till pole release<sup>4</sup>. This is due to motion of the point mass relative to the pole that cannot be implemented as time based. It depends on properties of the pole such as the pole's length and stiffness—these properties, however, are to be varied during the simulations.

## 2.2 Finite element model of the pole

Modern, elite vaulting poles are manufactured out of lightweight materials consisting mainly of glass fiber-reinforced plastics. The fiberglass pole is rolled on a mandrel and, subsequently, wrapped to stiffen the pole. The perfect

<sup>4</sup> Ekevad and Lundberg [11] control the vaulter motion by the angle  $\varphi$ . This leads to instabilities from the instance of maximum pole bending to pole release where the vaulter movement changes, based on the almost constant angle  $\varphi$ . Ekevad and Lundberg [11] tried to overcome this drawback by calculating an average rate of the change of the angle  $\varphi$  in the first half and applying this for the second half. Their approach is non-physical: the stretching of the pole is not coupled to the relative motion of the vaulter.

**Fig. 4** Positions of the vaulter's body segments and mass center (blue square) during different phases of the pole vault. Coordinate system  $x_1$ - $y_1$  is chosen for the presentation (color figure online)



pole differs for athletes, depending on their physical properties, abilities and vaulting technique- and plays an essential role in the vaulter's performance.

As a first step, an isotropic hyperelastic material model of Neo-Hookean type was applied with the strain-energy function

$$\Psi = \frac{\mu}{2} \left[ I_1(\hat{\mathbf{b}}) - 3 \right] + \frac{\kappa}{2} [J - 1]^2, \quad (2)$$

where  $\mu$  is the shear modulus,  $I_1 = \text{tr}(\hat{\mathbf{b}})$  is the first invariant of  $\hat{\mathbf{b}}$ ,  $\hat{\mathbf{b}} = J^{-2/3}\mathbf{b}$  is the distortional component of the left Cauchy–Green strain tensor,  $\kappa$  is the bulk modulus and  $J$  is the determinant of the deformation gradient  $\mathbf{F}$ . Neo-Hookean hyperelasticity renders linear elasticity as long as it is valid but also allows for nonlinear behavior which occurs due to the large deflection of the pole. Therefore, it is the more general choice. The material

density  $\rho$  and the Poisson's ratio  $\nu$  were calculated with the rule of mixtures (following [13]) for a fiber volume fraction of 50% as in Davis and Kukureka [14]. The modulus of elasticity was obtained via a flex test simulation<sup>5</sup>. This kind of test is used in the pole industry to classify the stiffness of a pole. The pole is pin-supported at both ends and loaded with a mass of 22.7 kg in the center. The deflection in cm gives the flex number (a relative stiffness number) of the pole. The assumed geometry of the equipment, namely the pole, is shown in Fig. 5. Table 2 summarizes the chosen properties. In the study on the pole stiffness (see Sect. 3), the elastic modulus is varied in the neighborhood of the previously calculated value of the flex test.

We discretized the pole with continuum elements as well as beam elements and compared the outcome. Continuum elements can represent arbitrary structures and bodies and can resolve complex three-dimensional stress states. Further, they allow for incorporating user defined material laws which might be desired when accounting for microstructure, for example. Structural elements such as beams rely on assumptions like slenderness simplifying the model to one predominant dimension. This leads to a reduced number of degrees of freedom and therefore, higher computational efficiency. ABAQUS' Timoshenko beam elements capture large axial strains [15].

### 2.3 Coupling of pole and vaulter

The point mass needs to be connected to the pole such that it can move relatively to the upper pole tip according to the vaulter's motion in different phases of the vault. Moreover, the connection fails once the pole is stretched and the vaulter would release it to clear the bar. An IAAF requirement is that the vaulter must hold the pole in the grip area (no higher than 0.1524 m from the top of any pole or no lower than 0.4572 m from the top of the pole).

ABAQUS' connector elements allow constraints involving relative motion of the connected parts via Lagrange multipliers as additional solution variables and also failure of the connection [15]. Through the connector element, a relative position of the point mass was given as a constraint on the upper tip of the pole. Moreover, the connector elements were employed as a sensor to measure the position  $[x_p, y_p]^T$  of the upper pole tip and the height  $h_m$  of the mass center. A user subroutine UAMP was used in each increment of the calculation to call the quantities measured by the sensors and enforce relative displacement components [16].

<sup>5</sup> This only holds true as long as the pole is modeled with constant cross-section and homogeneous material.

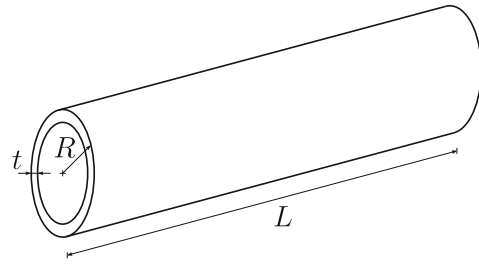


**Fig. 5** Dimensions of the pole: a tube like structure of length  $L$  featuring a hollow cross-section with radius  $R$  and wall thickness  $t$

In the UAMP routine, the pole angle  $\varphi$  and the relative height  $h_{m,rel}$  of the mass center were calculated via

$$\varphi = \arcsin\left(\frac{y_p}{\sqrt{x_p^2 + y_p^2}}\right) \quad \text{and} \quad h_{m,rel} = \frac{h_m}{L}. \quad (3)$$

As the sensor measurements are from the beginning of the time increment, the corresponding values of  $\varphi$  and  $h_{m,rel}$  at the end of the time increment were extrapolated. Subsequently, the relative position of the point mass in coordinate system  $x_2$ - $y_2$  in the next time step was determined as:

$$\begin{bmatrix} x_m \\ y_m \end{bmatrix} = \begin{cases} f(\varphi) & \text{if } \varphi \leq 60^\circ \\ f(h_{m,rel}) & \text{else,} \end{cases} \quad (4)$$

depending on the simulation state being in the first or the second part of the vault. Here,  $f$  is a function that interpolates the relative position of the point mass from the discrete values of the different phases that were obtained in Sect. 2.1. The values calculated with Eq. (4) were further used as an input to feed-forward control the relative motion of the point mass. The UAMP was employed to enforce the relative motion of the point mass until a relative height  $h_{m,rel}$  was reached, corresponding to the instance when the pole was completely recovered. Then, the connector fails corresponding to the vaulter releasing the pole. The push-off motion of the vaulter is negligible compared to the catapult effect of the pole [17]—regarding the current accuracy of the model. For a fully detailed model, the push-off angle of the vaulter should be taken into account. Eventually, the point mass moves freely under the influence of gravity only.

### 2.4 Initial and boundary conditions of pole vaulting

Regarding the boundary conditions of the simulation, the pole was supported at the lower end fixing all translational degrees of freedom. This represents the contact to the planting box. Furthermore, a gravitational acceleration of  $g = 9.81 \text{ m s}^{-2}$  was assumed.

The choice of the initial conditions is not trivial and has to be done carefully. Frequently reported in the literature, is

**Table 2** Summary of the properties of the pole

Property	Symbol	Value	Ref.
Length	$L$	4200 mm	[14]
Outer radius	$R$	21 mm	
Wall thickness	$t$	2.5 mm	
Density	$\rho$	1887.5 kg m <sup>-3</sup>	
Poisson's ratio	$\nu$	0.285	
Modulus of elasticity	$E$	37.5 GPa	
Flex number		15	

the employment of only the take-off velocity  $v_0$  on the vaulter (see e.g., [9, 11, 18]), while no initial velocity was applied to the pole. The initial velocity of the vaulter is split into two components: one in the horizontal direction due to the approach speed and one in the vertical direction due to the jump. The components are calculated with the take-off angle  $\alpha$ . Table 3 summarizes exemplary values for initial conditions according to Linthorne [18].

Due to the ‘hard contact’ boundary condition at the lower end, such an initial condition results in artificial oscillations of the pole with large amplitudes. All modes of the pole, which is initially at rest, are excited by the impulse. To circumvent these artificial oscillations, we started the simulation at the instance right after the pole was planted and when it started to bend as the vaulter's mass compressed it. Then, in addition to the initial velocity of the point mass, also a velocity profile  $v_{0,\text{pole}}$  on the pole was necessary that induced the bending. This profile was obtained from a preliminary simulation.

In this preliminary simulation, only the take-off velocity  $v_0$  of the point mass was applied as an initial condition and the density of the pole was artificially reduced by six orders of magnitude. Therefore, the oscillations still occurred in the beginning of the simulations but the amplitudes were small since the pole had nearly no inertia associated with it. In the following, the oscillations decayed quickly (approximately 0.01 s) and a homogeneous velocity profile developed in the pole (cf. Fig. 6).

The profile has velocity components in the horizontal and vertical directions and is not necessarily perpendicular to the pole. This profile was then extracted and employed as the initial condition for the simulation. The velocity profile's shape resembles the bending of the pole in its first mode. Thus, an initial velocity profile initiates the real deformation. In the pole vaulting simulation, the profile was approximated with a third order polynomial along the pole length  $L$  requiring:

1. Zero velocity at the lower end,
2. Velocity at the upper tip equals the preliminary simulation,

**Table 3** Initial conditions of the simulations

Initial condition	Symbol	Value
Take-off angle	$\alpha$	18°
Take-off velocity	$v_0$	8 m s <sup>-1</sup>
Horizontal component	$v_{0,x}$	7.608 m s <sup>-1</sup>
Vertical component	$v_{0,y}$	2.472 m s <sup>-1</sup>

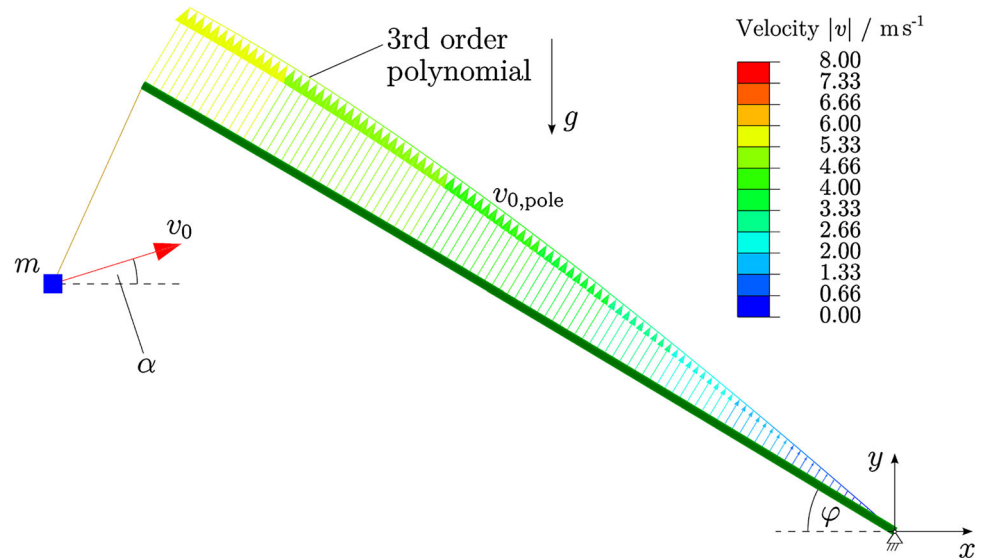
3. Maximum velocity node position matches the preliminary simulation, and
4. Maximum velocity value equals the preliminary simulation.

### 3 Results and discussion

Figure 7 illustrates sequential frames of the pole vault simulation. We investigated the influence of the effective bending stiffness  $EI_{\text{eff}}$  on the achievable vaulting height. The elastic modulus  $E$  was varied from 30 to 45 GPa (resulting in an effective bending stiffness range of 1822.42–2733.63 N m<sup>2</sup>) while all other material and geometry parameters of the pole were kept constant.

IAAF [19] demands the crossbar, that needs to be cleared, to be straight above the planting box or up to 0.8 m behind it. Thus, in the  $x$ - $y$  coordinate system from Fig. 2, the vault height  $h_{\text{max}}$  should be attained at an  $x$ -position in the range of 0.0–0.8 m. Therefore, pole vault attempts, where the  $x$ -position of the vaulter at the vault height  $h_{\text{max}}$  is negative, are considered to be a failed trial. Figure 8 depicts the maximum heights  $h_{\text{max}}$  of the point mass depending on the effective bending stiffness  $EI_{\text{eff}}$ . Valid trials are indicated with a green square whereas failed trials are displayed with a red triangle. The general trend of a higher effective bending stiffness leading to an increased height is observable. However, if the pole is too stiff, the vaulter is not able to bend the pole in such a way that he is catapulted forward-leading to a failed approach. The  $x$ -position at the height is illustrated in addition to signify valid and failed trials. The maximum height that is achieved in a valid trial is  $h_{\text{max}} = 7.58$  m with an effective bending stiffness of the pole of  $EI_{\text{eff}} = 2218$  N m<sup>2</sup>, corresponding to an elastic modulus of  $E = 36.52$  GPa. Considering that only the vaulter's body, but not his/her center of gravity, needs to pass the bar, slightly higher heights are possible. External circumstances as well as the fact that an athlete is never a perfect machine will decrease the realistic value. These results correspond well with world records. However, since dissipative effects are neglected, the computed height is slightly larger. The kinetic energy dissipated in the form of heat through the vaulter's muscles significantly influences the maximum height  $h_{\text{max}}$  [18]. In

**Fig. 6** Initial and boundary conditions of the simulation. The initial velocity profile is computed in a preliminary simulation



addition, the vaulter dissipates energy with impact when the pole is planted. The impact forces increase with higher pole stiffness. Since the simulation starts after the pole planting, this dissipation is as well neglected which especially influences the simulation outcome with poles of higher stiffness. Moreover, energy is dissipated due to friction at the planting box and the viscoelastic properties of the pole [20]. Further no force and momentum restrictions were considered for the relative movement of the mass point, meaning limits of human muscular strength are neglected at this stage. Essentially, computational simulations can compare different poles (i.e., different materials, lengths) as well as support the development of new poles.

The velocity of the point mass is displayed in Fig. 9. The velocity  $v_x$  in the horizontal direction decreases in the beginning as the kinetic energy of the approach is transferred into strain energy by deforming the pole. Subsequently, the velocity  $v_y$  in the vertical direction increases when the pole recovers to catapult the vaulter. After releasing the pole, the horizontal velocity  $v_x$  is constant since no forces act on the point mass in that direction. Contrary, the upward vertical velocity  $v_y$  of the vaulter decreases linearly under the effect of gravity. When the vertical velocity  $v_y$  decreases to zero, the maximum height  $h_{\max}$  and accordingly the maximum potential energy is reached. The energy transformations correspond well to the experimentally based descriptions of Dillmann and Nelson [21]. The simulated velocities correspond well in trend and magnitude to the measured ones of Frère et al. [4] and Angulo-Kinzler et al. [22].

### 3.1 Finite element choices: continuum vs. beam elements

The aim of this contribution was to allow for more detailed material models taking into account the heterogeneity of

fiber-reinforced plastics. If the pole's heterogeneous microstructure is to be taken into account, continuum elements<sup>6</sup> need to be applied. They are computationally more costly, but distributions of field variables can be identified precisely and they allow to account for a sophisticated microstructured material model at a later stage.

If the underlying pole material is treated as a homogeneous continuum, the pole can be discretized with beam elements<sup>7</sup>. The use of beam elements is suitable since the pole has only one dominant dimension whereas the other two are relatively small. The advantage of this approach is its computational cheapness allowing fast model studies. Thus, beam elements were used for the simulations in the effective bending stiffness study performed in this work and the microstructure was neglected. For reasons of comparison, the performance of beam vs. continuum elements is illustrated exemplarily for one case in Fig. 9.

## 4 Conclusion

This study provides a framework for FE simulations of pole vaulting, suitable for investigations on the pole's material. The vaulter was accounted for as a point mass to

<sup>6</sup> ABAQUS' C3D8R continuum elements (8 nodes with 3 displacement degrees of freedom per node and linear shape functions) were applied in this case [15]. These elements possess one Gaussian integration point. Reduced integration was used to avoid shear locking. For such elements, artificial hourglass deformation modes may occur. The occurrence of these modes was controlled via the artificial strain energy that has to be small compared to the strain or internal energy.

<sup>7</sup> ABAQUS' B21 beam elements were employed which are located in 2D space and use linear shape functions [15]. They possess two nodes with three degrees of freedom each (two displacements and one rotation) and two integration points. Timoshenko beam formulation was utilized.

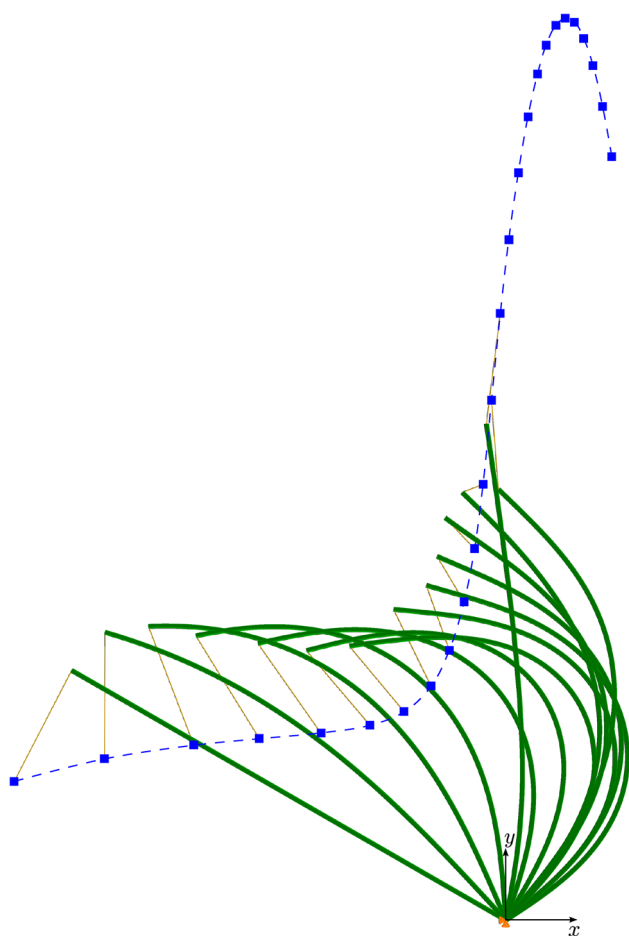


**Fig. 7** Deformation of the pole and motion of the point mass: The point mass is depicted by a blue square. The thin orange line indicates the coupling of the point mass to the pole via the connector element and, by that, its relative movement. The trajectory of the point mass is illustrated by the dotted line. After the pole is recovered and the vaulter releases the pole, only the point mass is shown (color figure online)

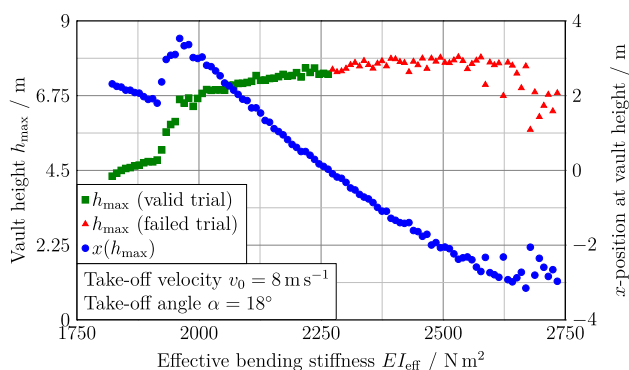


**Fig. 8** Maximum height  $h_{\max}$  of point mass and corresponding  $x$ -position depending on the effective bending stiffness  $EI_{\text{eff}}$  of the pole material

save computational effort in control that was necessary in other studies. The motion of the vaulter relative to the pole was implemented with an algorithm based on a reference

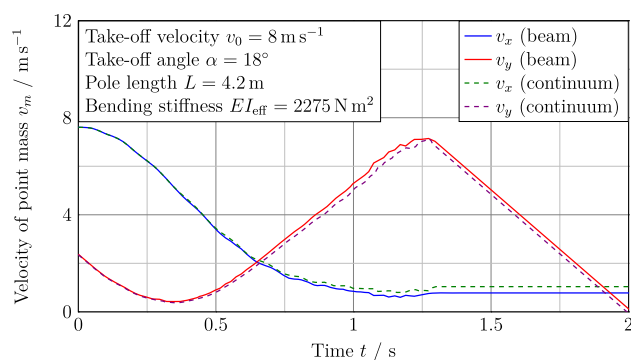


**Fig. 9** Velocity of point mass over time. Discretizations with (1) beam and (2) continuum elements

vault of an elite pole vaulter. The focus was on the proper choice of boundary and initial conditions to avoid unphysical oscillations. An initial velocity profile of the pole was determined by running a pre-simulation with reduced pole weight and overcomes unnatural simulation outcomes.

Beam elements as well as continuum elements can be used for the discretization of the pole yielding similar results. Continuum elements give a more detailed insight in distributions of field variables such as stresses and strains. Furthermore, they provide the option to study and incorporate complex computationally expensive material models considering the micromechanical structure of the pole.

The simulation results resemble measurements of the pole vault process in trend and magnitude. Additionally, we examined the influence of the effective bending stiffness of the pole on the achievable height in pole vaulting using an isotropic Neo-Hookean (continuum elements)/linear elastic (beam elements) material model and varying the elastic modulus. We observed that up to a certain stiffness, higher effective bending stiffness leads to higher pole vaulting heights. However, overly stiff poles would not bend enough to catapult the vaulter forward leading to failed vault attempts. This naturally occurring phenomenon is well reflected in our model.

**Open Access** This article is distributed under the terms of the Creative Commons Attribution 4.0 International License (<http://creativecommons.org/licenses/by/4.0/>), which permits unrestricted use, distribution, and reproduction in any medium, provided you give appropriate credit to the original author(s) and the source, provide a link to the Creative Commons license, and indicate if changes were made.

## References

- Griffin S (2016) Pole vaulting history. url: <http://www.livestrong.com/article/353272-pole-vaulting-history/> (visited on 05/07/2016)
- International Association of Athletics Federations (2016) Pole vault. url: <http://www.iaaf.org/disciplines/jumps/pole-vault> (visited on 05/07/2016)



3. Hirn H (2015) Sportrekorde-Leichtathletik. url: [http://rekorde-im-sport.de/Leichtathletik/maenner\\_stabhochsprung.html](http://rekorde-im-sport.de/Leichtathletik/maenner_stabhochsprung.html) (visited on 10/08/2015)
4. Frère J, L'Hermette M, Slawinski J, Tourny-Chollet C (2010) Mechanics of pole vaulting: a review. *Sports Biomech* 9(2):123–138
5. Arampatzis A, Schade F, Brüggemann GP (2004) Effect of the pole-human body interaction on pole vaulting performance. *J Biomech* 37(9):1353–1360
6. Frère J, Göpfert B, Slawinski J, Tourny-Chollet C (2012) Effect of the upper limbs muscles activity on the mechanical energy gain in pole vaulting. *J Electromyogr Kinesiol* 22(2):207–214
7. Morlier J, Mesnard M (2007) Influence of the moment exerted by the athlete on the pole in pole-vaulting performance. *J Biomech* 40(10):2261–2267
8. McGinnis PM (1997) Mechanics of the pole vault take-off. *New Stud Athl* 12(1):43–46
9. Ekevad M, Lundberg B (1997) Influence of pole length and stiffness on the energy conversion in pole-vaulting. *J Biomech* 30(3):259–264
10. Hubbard M (1980) Dynamics of the pole vault. *J Biomech* 13(11):965–976
11. Ekevad M, Lundberg B (1995) Simulation of 'smart' pole vaulting. *J Biomech* 28(9):1079–1090
12. Schade F, Arampatzis A, Brüggemann GP (2000) Influence of different approaches for calculating the athlete's mechanical energy on energetic parameters in the pole vault. *J Biomech* 33(10):1263–1268
13. Zenkert D, Battley M (2003) Foundations of fibre composites. KTH Royal Institute of Technology, Stockholm
14. Davis CL, Kukureka SN (2012) Effect of materials and manufacturing on the bending stiffness of vaulting poles. *Phys Educ* 47(5):524–529
15. Dassault Systèmes (2012) Abaqus 6.14 analysis user's manual. Dassault Systèmes Simulia Corp., Providence
16. Dassault Systèmes (2012) Abaqus 6.14 user subroutines reference guide. Dassault Systèmes Simulia Corp., Providence
17. Frère J, Göpfert B, Hug F, Slawinski J, Tourny-Chollet C (2012) Catapult effect in pole vaulting: Is muscle coordination determinant? *J Electromyogr Kinesiol* 22(1):145–152
18. Linthorne NP (2000) Energy loss in the pole vault take-off and the advantage of the flexible pole. *Sports Eng* 3(4):205–218
19. International Association of Athletics Federations (2013) Competition rules 2014–2015. International Association of Athletics Federations (IAAF), Monaco
20. Schade F, Arampatzis A, Brüggemann GP (2006) Reproducibility of energy parameters in the pole vault. *J Biomech* 39(8):1464–1471
21. Dillman CJ, Nelson RC (1968) The mechanical energy transformations of pole vaulting with a fiberglass pole. *J Biomech* 1(3):175–183
22. Angulo-Kinzler RM, Kinzler SB, Balias X, Turro C, Caubet JM, Escoda J, Prat JA (1994) Biomechanical analysis of the pole vault event. *J Appl Biomech* 10(2):147–165